A Thesis for the Degree of Master of Science

Study on parameters for aggregation and precipitation in the switchable-linker based detection system using gold nanoparticles

금나노 입자를 이용한 switchable-linker 기반 검출법의 응집과 침전반응에 영향을 미치는 요소에 관한 연구

August, 2018

Jaeyeon Kim

Department of Agricultural Biotechnology

Seoul National University

농학석사학위논문

Study on parameters for aggregation and precipitation in the switchable-linker based detection system using gold nanoparticles

금나노 입자를 이용한 switchable-linker 기반 검출법의 응집과 침전반응에 영향을 미치는 요소에 관한 연구

지도교수 최영진

이 논문을 석사학위 논문으로 제출함

2018년 8월

서울대학교 대학원 농생명공학부

김 재 연

김재연의 석사 학위논문을 인준함

2018년 8월

위원장 최상호 (인)

부위원장 최영진 (인)

위원 이기원 (인)

ABSTRACT

Aggregation of gold nanoparticles (AuNPs) has been used in various fields for assorted purposes. In particular, detection of analytes through visual color changes induced by aggregation of AuNPs has been extensively studied in recent years. In our previous research, switchable-linker based detection system was introduced. In the system, sensing of specific targets is achieved based on the quantitative correlations between linkers, targets and particles. When the number of particles and linkers are ideally matched, a maximum aggregation occurs in suspension inducing aggregates settling. This linker range where aggregates precipitation dominantly occurs is called 'exhibiting visual color change (REVC)'. Since REVC plays a critical role in the system, it is important to gain an understanding of the factors that could affect in REVC formation. However, little research has been done about the basic mechanisms of REVC formation based on AuNPs aggregation and precipitation, especially focusing on the effects of particles' size and surface area.

In this study, the effects of total surface area of AuNPs in REVC formation were identified by comparing 3 different cases. In the first case, 11 nm and 19 nm-sized particles were used in the previous study. Under the same plasmon absorbance, as the size of particle increased, the total surface area

decreased. In this case, REVC appeared at lower linker concentrations with a narrower range. After the addition of target streptavidin, REVC shifted more in 19 nm particles which had smaller surface area. As for the second case, 12, 18, and 24 nm-sized particles were used. In this case, the number of particles was identically adjusted, thus as the particle size increased, the total surface area of AuNPs increased. In larger surface area, REVC appeared at higher linker concentrations in a broader range which correspondsss to the previous results. With the addition of target streptavidin, REVC shifted less as the surface area increased. Lastly, the surface area of AuNPs was identically adjusted by controlling the number of particles using 13, 21, 30, and 36 nm-sized particles. Under the same surface area, REVC was formed at a similar linker concentrations regardless of individual particle sizes and REVC shifting occurred identically under the addition of target streptavidin. Three cases indicated that as the surface area of AuNPs decreased, REVC worked more sensitively as a sensor.

As part of an effort to confirm the reaction time according to particles, the third case was intensively interpreted. When the surface area of AuNPs was identically controlled, it was observed that in 21 nm-sized particles, REVC was formed the slowest among others in observation time of 200 minutes. From DLS size measurements of aggregates and Stokes' law, settling velocity of aggregates in REVC was calculated. At an early settling stage,

aggregates of 30 and 36 nm-sized particles precipitated more rapidly. However, as time went by, settling speed of aggregates composed of 13 and 21 nm-sized particles reached beyond the speed of larger particles. At around 120 minutes, the settling velocity of aggregates composed of 13 nm-sized particles went over than that of 21 nm-sized particles. This phenomenon might be explained by the fact that smaller individual particles made clusters more rapidly in much bigger sizes, thus settling speed inversion seemed to be happened.

The results of this study suggest the importance of the surface area in REVC formation and the aggregates precipitation speed inversion was revealed by the actual calculations using Stokes' law. These can be contributed to the further development of switchable-linker based detection system and can be used as clues in other aggregation-based applications.

Keywords: gold nanoparticles, size, surface area, aggregation, settling velocity, REVC, switchable-linker

Student Number: 2016-25275

CONTENTS

LIST OF FIGURES

LIST OF TABLES

Ⅰ. INTRODUCTION

In various fields including bio-medical, environment relevancy, and food safety, a fast and reliable detection for specific targets which is also inexpensive, simple-to-perform, and no need for trained technique has been highly on demand (Ai, Liu, & Lu, 2009; Liu et al., 2013; Shrivas, Shankar, & Dewangan, 2015; Wang, Lee, & Lu, 2008). Amongst assorted detection systems, colorimetric assays have appreciable possibilities as on-site sensor since visual color changes can be identified with naked eyes, and therefore no affiliated instruments are required (Vilela, González, & Escarpa, 2012; Zhao, Ali, Aguirre, Brook, & Li, 2008).

Gold nanoparticles (AuNPs) are considered as apposite tool for colorimetric assays due to their unique optical properties (Nath & Chilkoti, 2002). Especially, much research has been done about AuNPs' aggregation-based applications.

In our previous research, fast and sensitive colorimetric detection using switchable linkers (biotinylated BSA, bBSA) and AuNPs was suggested (Lim et al., 2012). The overall reaction is composed of 2 basic mechanisms which are the aggregation of particles and clusters' precipitation. Briefly,

streptavidin-functionalized gold nanospheres are linked by switchable linkers (bBSA), and at certain linker concentrations, a large-scale aggregation of AuNPs occurs inducing aggregates precipitation making the red wine color of colloidal gold transparent. We called the regions where large-scale aggregations occur followed by aggregates precipitation as 'exhibiting visual color change (REVC)'. When specific targets (streptavidin as a model target) are added, REVC moves to higher linker concentrations because added targets bind to switchable linkers thus more linkers are needed to trigger the same scale of aggregation. Since REVC is regarded as a core factor in the switchable-linker based detection system, research of adjusting and controlling REVC has always been on demand. Using the system, we have achieved an ultra-sensitive visible detection of *Salmonella* in *tomato* (Hahn et al., 2017), and peanut allergen Ara h1 in peanut extract (Kim, 2016).

According to our previous research, by intentionally reducing the number of streptavidin coated on the surface of AuNPs, the number of linkers needed for REVC formation decreased (Kim, 2016). As a sensor system, when REVC is formed at a lower linker range, it is considered as more efficient since fewer linkers are consumed in order to trigger the optimal aggregation. In addition, we empirically identified that when the total surface area of AuNPs decreased, the amount of linkers for REVC formation also decreased.

From these previous studies, it is assumed that total surface area of AuNPs would play an important role in the formation of REVC. However, no direct research has been done about how surface area of AuNPs would affect the REVC formation and overall detection system in terms of reaction time.

In this research, 3 different cases when the total surface area of AuNPs was reduced, increased, and identically adjusted were identified in order to verify the effects of surface area in REVC formation. In addition, aggregates properties in REVC of 4 different particles under the same surface area in terms of aggregates settling velocity were investigated based on the size measurements, and a settling speed inversion between 13 and 21 nm-sized particles was confirmed as a basis of Stokes' law.

By exploring the influence of surface area with different size, this research aims to set forth to provide an actual data of the importance of surface area and AuNPs size in REVC formation and expected to be used as a useful reference for the aggregation-based applications with particle surface modification in many fields.

Ⅱ. MATERIALS AND METHODS

2.1. Materials

Hydrogen tetrachloroaurate trihydrate ($HAuCl_4$ $3H_2O$, ≥ 99.99%), streptavidin from Streptomyces, albumin (biotin labeled bovine) were purchased from Sigma-Aldrich. Tri-Sodium citrate·2hydrate ($Na_3C_8H_5O_7 \cdot 2H_2O$ ≥ 99.99%) was purchased from Yakuri Pure Chemicals Co., Ltd (Kyoto, Japan). Tetraborate pH standard solution was purchased from Wako Pure Chemicals Industries, Ltd (Osaka, Japan). Phosphate Buffered Saline (PBS) was purchased from Thermo Fisher Scientific (Waltham, MA, USA). Milli-Q water of 18.2 MΩ.cm was used in all experiments. All glassware was cleaned with aqua regia.

2.2. Instrumentation

Transmission electron microscopy (TEM) was performed with a Gatan transmission electron microscope. Sample was prepared by dropping 10 μL onto a carbon-coated grid. The grid was subsequently dried in air and then imaged. A Zetasizer Nano ZS system (Malvern) Dynamic Light Scattering

Detector was used for the dynamic light scattering (DLS) measurements. The DLS instrument was operated under the following conditions: temperature 25 ℃, detector angle 90, incident laser wavelength 632.8 nm and laser power 22 mW. The DLS data were processed using DTS 5.1 software. Samples for DLS analysis were diluted with 1.0 mL ultrapure water to the appropriate concentration, mixed well and left to stand for 2 min before each measurement. UV-visible absorption spectra were recorded using a quartz cell (1 mm path length). The samples were diluted 10 fold with distilled water.

2.3. Preparation of gold nanoparticles

Preparation of 12 and 13 nm GNPs. Colloidal golds were prepared by the citrate-mediated reduction of $HAuCl_4$ developed by Turkevich et al. Briefly, gold hydrochlorate solution (5 mL, 10 mM) was added to 45 mL of distilled water. The solution was heated until it started to boil followed by the addition of sodium citrate (5 mL, 38.8 mM) with vigorous stirring. In this mixing step, its color changed from pale yellow to bold red. The solution was cooled to room temperature. The size of AuNPs was about 13 nm as identified by TEM analysis and DLS measurements, the corresponding absorption peak was at 520 nm.

Preparation of 18, 21, 24, 30, and 36 nm GNPs. The larger sizes of AuNPs were prepared by stepwise seeded growth method with addition of sodium citrate and $HAuCl_4$ solution described by Bastus et al. Briefly, gold seeds were prepared by injecting $HAuCl_4$ (1 mL, 25 mM) into boiling sodium citrate solution (150 mL, 2.2 mM). The color gradually changed from faint pink to red-wine color within 10 minutes. After that, the temperature was cooled down to 90℃ in order to inhibit additional nucleation and to slow down the reaction. Once the temperature got stabilized, $HAuCl_4$ (1 mL, 25 mM) was added and stayed for 30 min with continuous stirring. Again, the same procedure was repeated. After that, the solution was diluted by extracting 55 mL of the solution and adding sodium citrate (2 mL, 60 mM) and 53 mL of distilled water. This solution was then used as seed solution and further steps were repeated until the particles reached to aimed size. The average size and its distribution was determined by TEM analysis and DLS as 18, 21, 24, 30, and 36 nm, corresponding absorption peak was at 522, 522.5, 524, 529 and 533 nm, respectively (Figure 1 and 2).

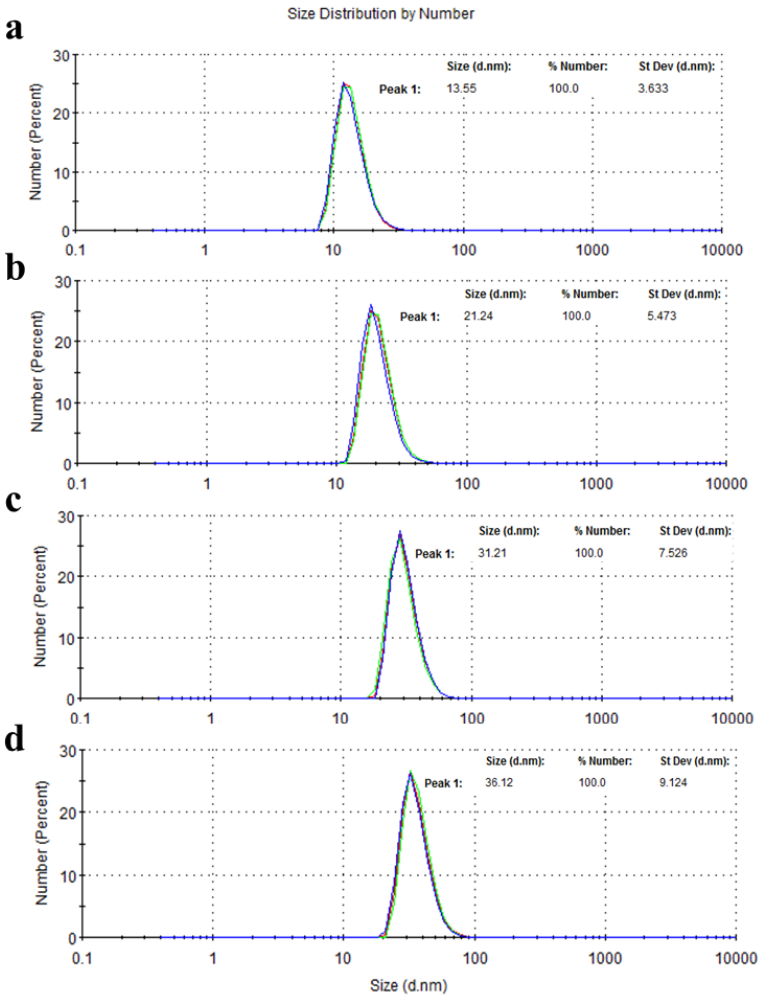

Figure 1. DLS size measurements of AuNPs; (a) 13 nm, (b) 21 nm, (c) 30 nm, (d) 36 nm. *Average diameter of 3 measurements, number-based data.

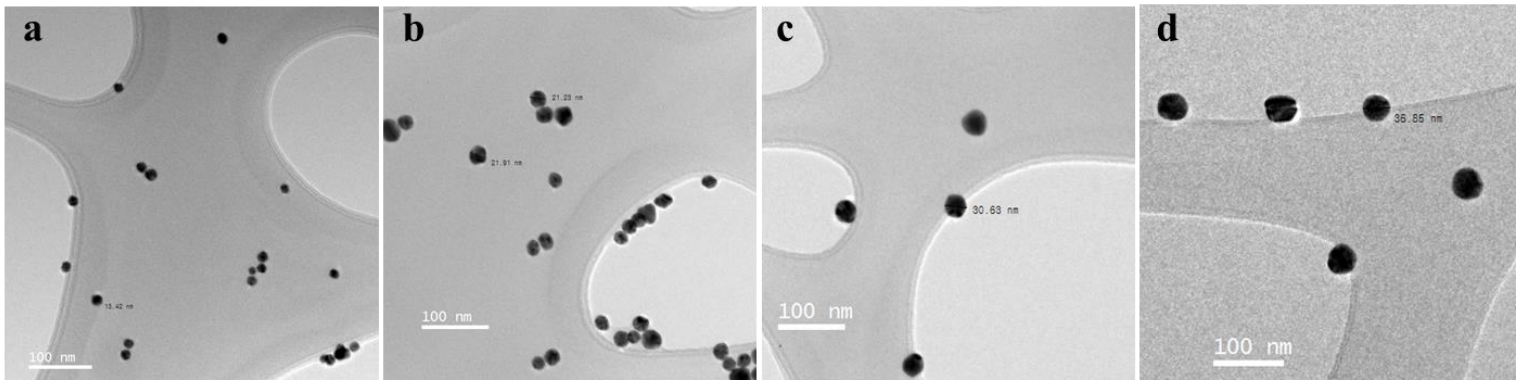

Figure 2. TEM images of AuNPs; (a) 13 nm, (b) 21 nm, (c) 30 nm, (d) 36 nm.

2.4. Preparation of streptavidin-coated gold nanoparticles (stAuNPs)

Citrate-stabilized AuNPs were coated with streptavidin in order to obtain colloidal stability and also to be used in streptavidin-biotin interaction. For 12-13 nm AuNPs coating, 1-40 μg/200 μL of streptavidin were rapidly added to 600 μL of AuNPs (λ_{max} at 520, absorbance value 0.2 at 1/10 dilution, 3.7 x 10^{12} particles/600 μL). For 21-24 nm AuNPs, 5-40 μg/200 μL of streptavidin were added to 600 μL of AuNPs (λ_{max} at 524, absorbance value 0.28 at 1/10 dilution, 5.52 x 10^{12} particles/600 μL). For 30-36 nm AuNPs (λ_{max} at 529-533, absorbance value 0.46 at 1/10 dilution, 4.03 x 10^{11} particles/600 μL), 20-200 μg/200 μL of streptavidin were used. The successful coating was identified using both plasmon peak shift and DLS analysis in each streptavidin concentration. After coating, the absorption peak was changed from 520 to 530 nm, 524 to 530 nm, and 529 to 538 nm, respectively (Figure 3-5).

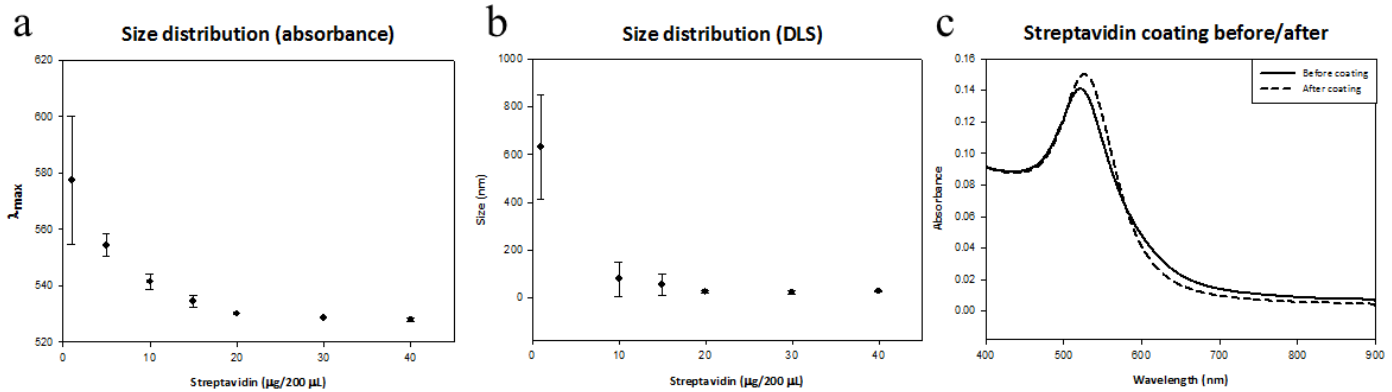

Figure 3. Size distribution data of 12-13 nm AuNPs based on the amount of streptavidin for surface full coverage; (a) Plasmon peak (λ_{max}), (b) DLS size distribution (number-based), (c) Absorption spectra changes before/after streptavidin addition.

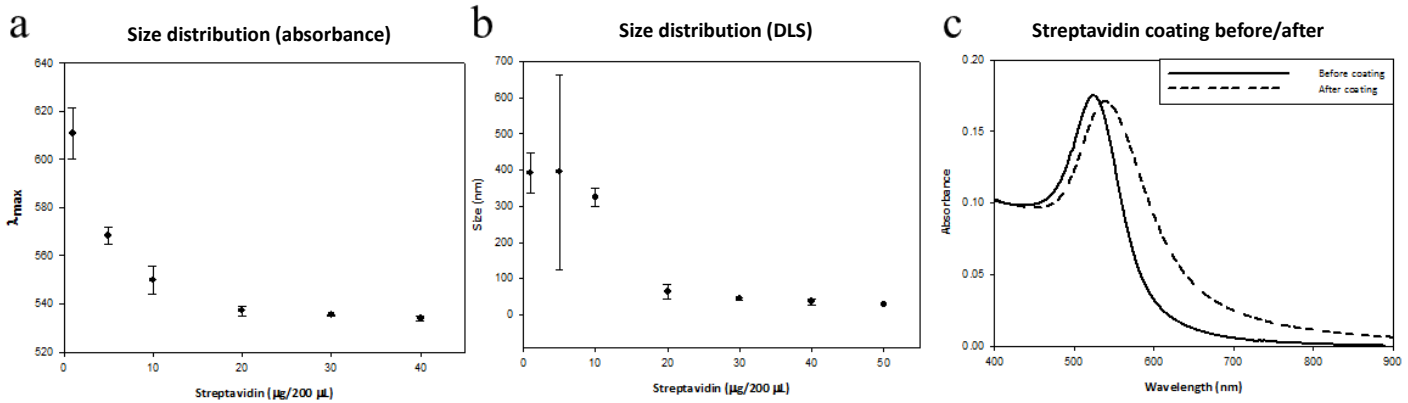

Figure 4. Size distribution data of 18-24 nm AuNPs based on the amount of streptavidin for surface full coverage; (a) Plasmon peak (λ_{max}), (b) DLS size distribution (number based), (c) Absorption spectra changes before/after streptavidin addition.

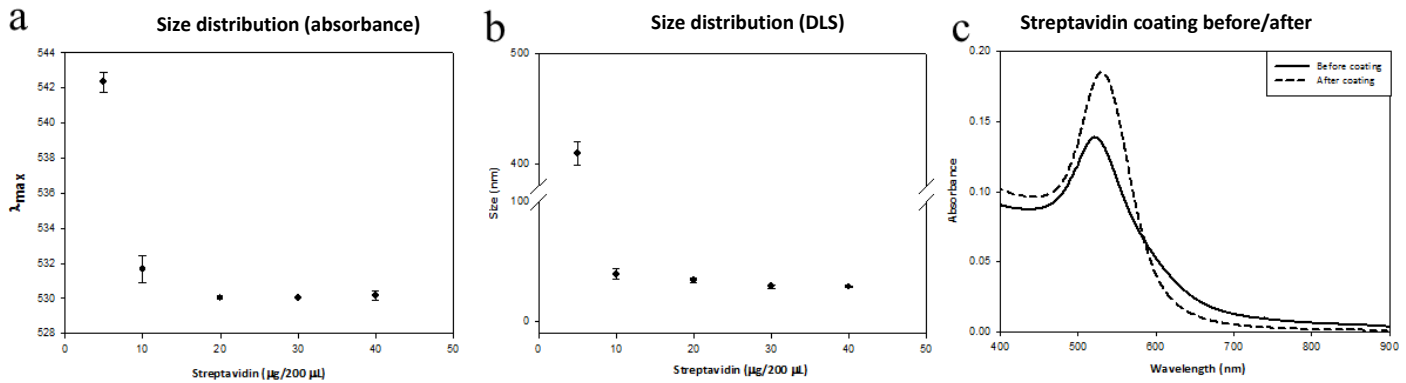

Figure 5. Size distribution data of 30-36 nm AuNPs based on the amount of streptavidin for surface full coverage; (a) Plasmon peak (λ_{max}), (b) DLS size distribution (number based), (c) Absorption spectra changes before/after streptavidin addition.

2.5. Adjustment of the total surface area of AuNPs

In order to identically adjust the total surface area of the different sized particles, the number of particles in 1 mL of colloidal gold was calculated based on the verifiable method by BBI corporations. Under the same absorption spectra which was at absorbance 1, the number of particles of 13, 21, 30, and 36 nm was 2.15×10^{12}, 5.7×10^{11}, 1.9×10^{11}, and 1.2×10^{11} ea/mL, respectively. Later on, total surface area/mL was calculated by multiplying the surface area of a single particle and the number of particles/mL. The overall calculated data was shown in Table 1.

Table 1. The number of particles and the total surface area in the same volume of different -sized colloidal gold.

	Particle diameter (nm)			
	13	**21**	**30**	**36**
***Surface area (nm^2)/ea particle**	530.7	1384.7	2826	4069.4
****ea particles/mL**	2.15×10^{12}	5.65×10^{11}	1.94×10^{11}	1.16×10^{11}
*****Total surface area (nm^2)/mL**	3.96×10^{14}	2.52×10^{14}	1.75×10^{14}	1.52×10^{14}
******Total surface area ratio based on 13 nm**	1	1.57	2.26	2.61
*******ea particle/mL**	4.3×10^{11}	1.8×10^{11}	8.8×10^{10}	6.1×10^{10}
Ratio	1	2.4	4.9	7

*-****: The data shown was based on the same absorption spectra, OD=1.

*****: The number of used particles for the reaction.

2.6. Schematic explanations of the switchable-linker based detection system

The switchable-linker based detection system is based on a reaction of three components which are switchable linkers, targets, and gold nanoparticles (Lim et al., 2012). In order to identify REVC without targets addition, a row of serial concentrations of switchable linkers is put in vials. When the optimal quantitative relationship between linkers and particles is satisfied, a maximum aggregation will be occurred with continuous precipitation in certain linker concentrations. Volume ratio of 3 components was kept constant in all experiments as follow; linkers : targets : particles = 1 : 1 : 2.

When specific targets are added (streptavidin in this case), switchable linkers bind to targets predominantly. Compared to the control batch in which no target is added, more switchable linkers are needed to trigger an optimal scale of aggregation for cluster precipitations. Thus, REVC shifts to higher linker concentrations, and we call this phenomenon “shifting”. By comparing the moved REVC before and after the target addition, this system acts as a strong visible sensor.

As shown in Figure 6, the reaction is mainly composed of two reactions which are aggregation of AuNPs and their ongoing precipitation. It

is considered that aggregation and precipitation overlaps each other (Figure 7). The velocity of each reaction could affect the overall reaction time.

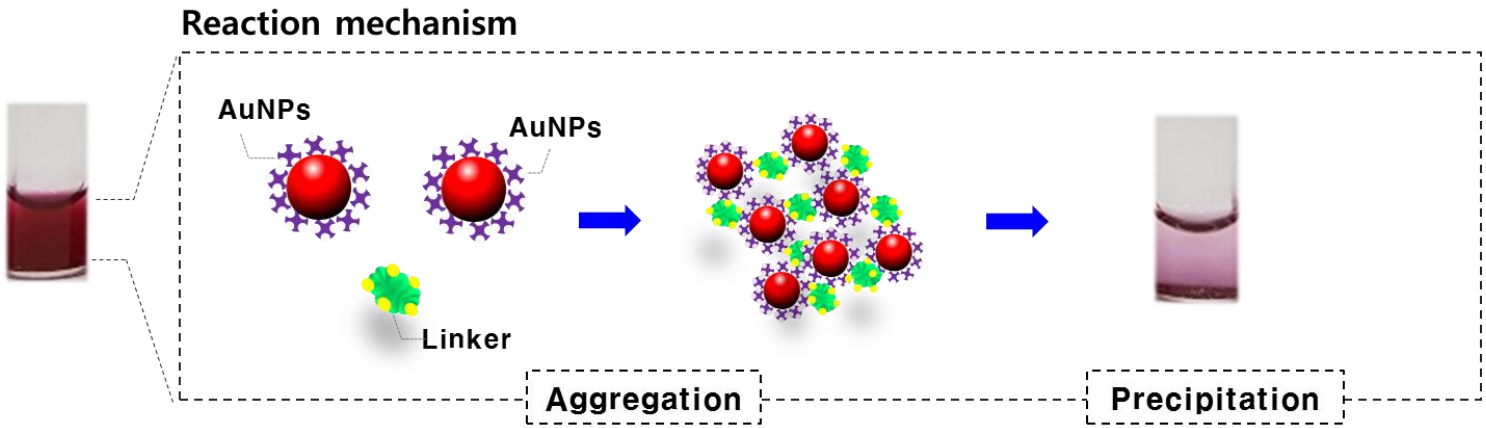

Figure 6. Schematic of switchable-linker based detection system.

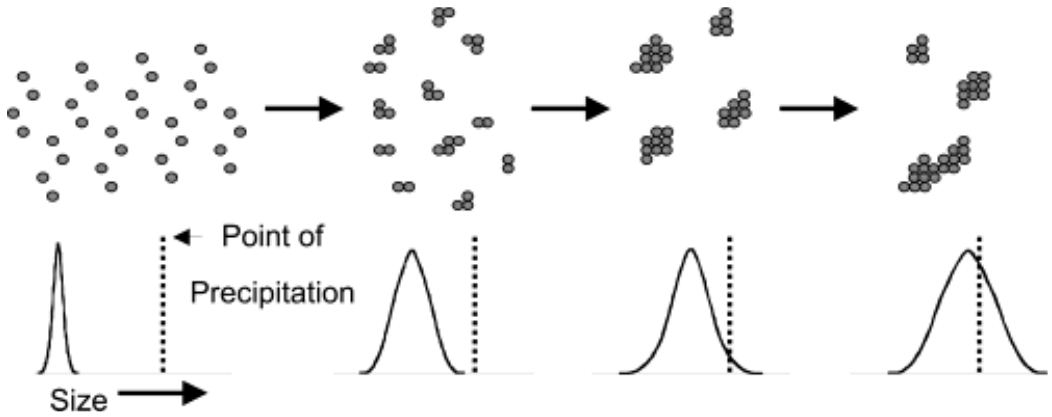

(Costanzo et al. *Chem. Mater*.2004)

Figure 7. Schematic of aggregation and precipitation occurring in REVC.

Ⅲ. RESULTS AND DISCUSSION

3.1. Effects of AuNPs surface area on REVC formation under the different conditions

In the switchable-linker based detection system, REVC stands for the regions where maximum aggregates are formed under the optimal linker-particle relationship. The range of linker concentrations where REVC is formed and the time that discernable difference appears are crucial factors in the system for further use as an on-site sensor. Amongst various factors, the effects of AuNPs surface area especially when it's decreased, increased, and same were compared to the control set and the REVC shifting under the addition of target streptavidin was compared as well.

3.1.1. REVC formation under the same absorption spectra

The first condition was conducted as follows in the previous research; when the absorption spectra of two different sized particles (11 and 19 nm) was identically adjusted as OD=0.4 (at 1/10 dilution), the number of particles decreased along with the total surface area as the particle size increased. In 11 nm-sized particles, the major REVC appeared at 0.6-1.0 μg/100 μL of linker

concentrations. In 19 nm-sized particles, REVC appeared at 0.4-0.6 μg/100 μL of linker concentrations (Figure 8). When REVC appears at lower linker concentrations, it is more desirable as a sensor, because it means that less linkers are needed to induce large scale aggregation, which is more effective. In addition, the range of REVC also indicates an important meaning as a sensor. When the range of REVC is narrow, more sensitive detection can be possible. When the target streptavidin was added, REVC with 19 nm-sized particles shifted more compared to 11 nm-sized particles under the same target concentrations. It meant that in smaller AuNPs surface area, the sensor released much amplified signal as in the form of REVC shifting (Figure 9).

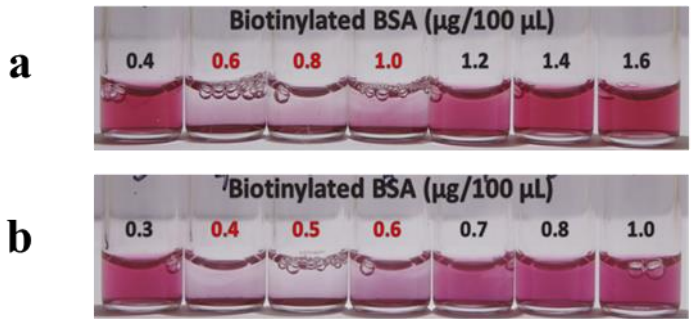

(Previous research, 2016)

Figure 8. Images of REVC formation; (a) 11 nm, (b) 19 nm.

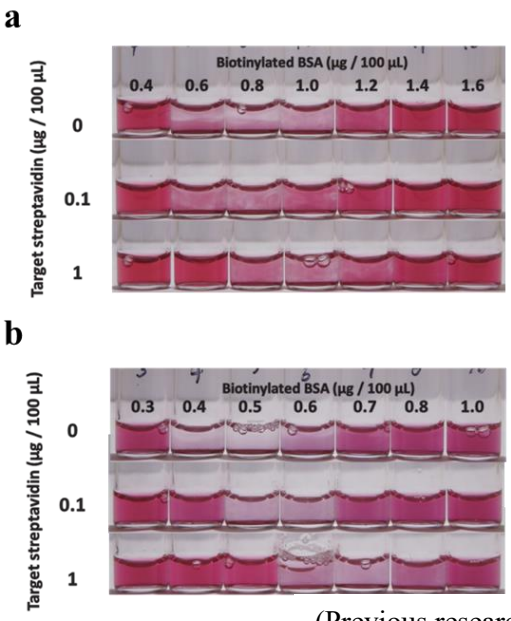

(Previous research, 2016)

Figure 9. Images of REVC shifting depends on the different concentrations of target streptavidin addition; (a) 11 nm, (b) 19 nm.

3.1.2. REVC formation under the same number of particles

In the second case, the number of particles was identically adjusted as 6.2 x 10^{12} ea/mL using 12, 18, and 24 nm-sized particles. Since the number of particles was same, the total surface area of AuNPs increased as the size of particles increased. In this case, REVC appeared at 0.5-0.7 μg/100 μL, 1.0-1.7 μg/100 μL, and 2-3.1 μg/100 μL of linker concentrations in 12, 18, and 24 nm-sized particles, respectively (Figure 10). It was verified that as the surface area of particles increased, the amount of linkers to induce maximum aggregation increased. This may be due to the fact that larger surface area consumed more linkers thus more linkers were required for the cluster formation. In addition, the range of REVC became wider, since there were more opportunities for the particles to make precipitation-possible clusters in broader linker concentrations. With the addition of target streptavidin, REVC shifted more in 12 nm and in the order of 18, and 24 nm-sized particles (Figure 11). It showed that as the surface area of AuNPs increased, REVC shifted less under the same target concentration, which was undesirable as a sensor.

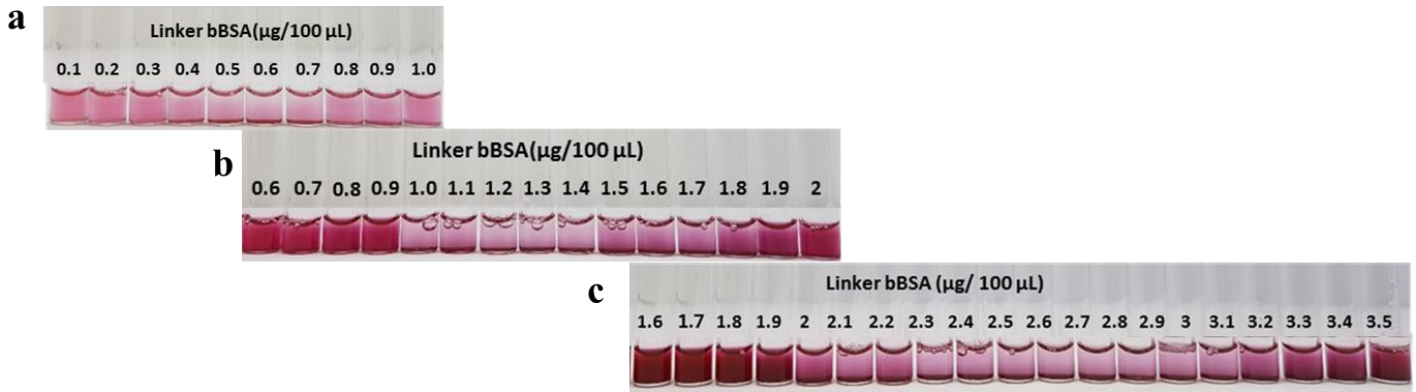

Figure 10. Images of REVC formation; (a) 12 nm, (b) 18 nm, (c) 24 nm.

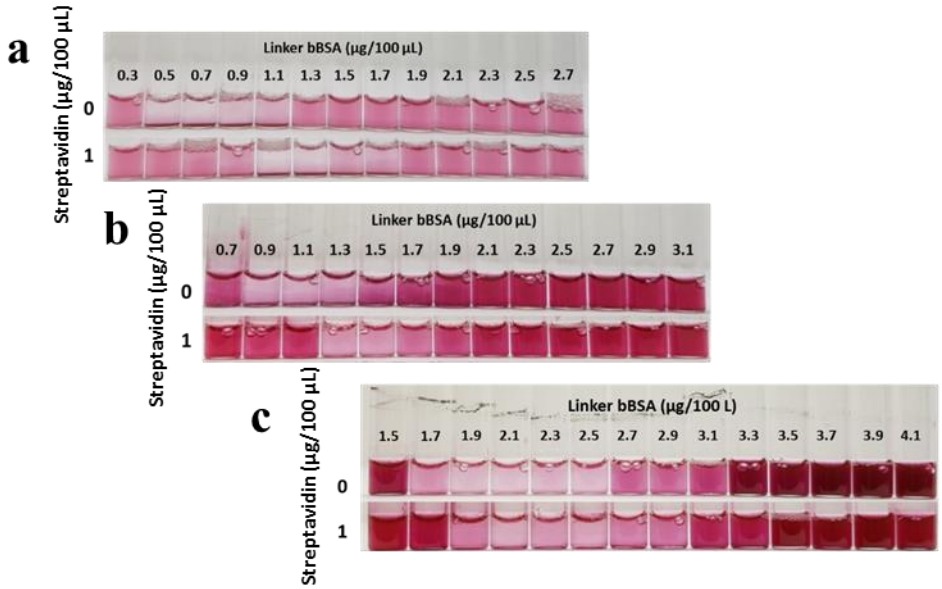

Figure 11. Images of REVC shifting depends on the target streptavidin addition; (a) 12 nm, (b) 18 nm, (c) 24 nm.

3.1.3. REVC formation under the same AuNPs surface area

When 13, 21, 30, and 36 nm-sized AuNPs have the same surface area, the REVC was formed at similar linker concentrations between 0.4-0.6 μg/100 μL and REVC shifted to the similar extent (Figure 12 and 13). It meant that similar amount of linkers was consumed to reach the maximum aggregation for REVC formation when the total surface area was identical.

Under the same AuNPs surface area, the number of particles in the same volume of colloidal gold was different, and increasing in effective particle size leading to decrease in overall particle numbers (Ferguson, Schultz, Rohatgi, & Kim, 2014). However, from this result, it was revealed that the ratio of AuNPs surface area and the amount of switchable linkers affected the REVC formation in different-sized particles with the same surface area. It can be explained as follows. Since the total surface area was identical in 4 different-sized particles, there must have been similar chances that switchable linkers could interact with AuNPs surface-coated streptavidin. In other words, the correlation between the amount of switchable linkers and surface area appeared as a form of REVC in the system, indicating that REVC where a maximum aggregation occurs is ultimately as a result of the optimal concentration ratio between AuNPs surface area and switchable linkers.

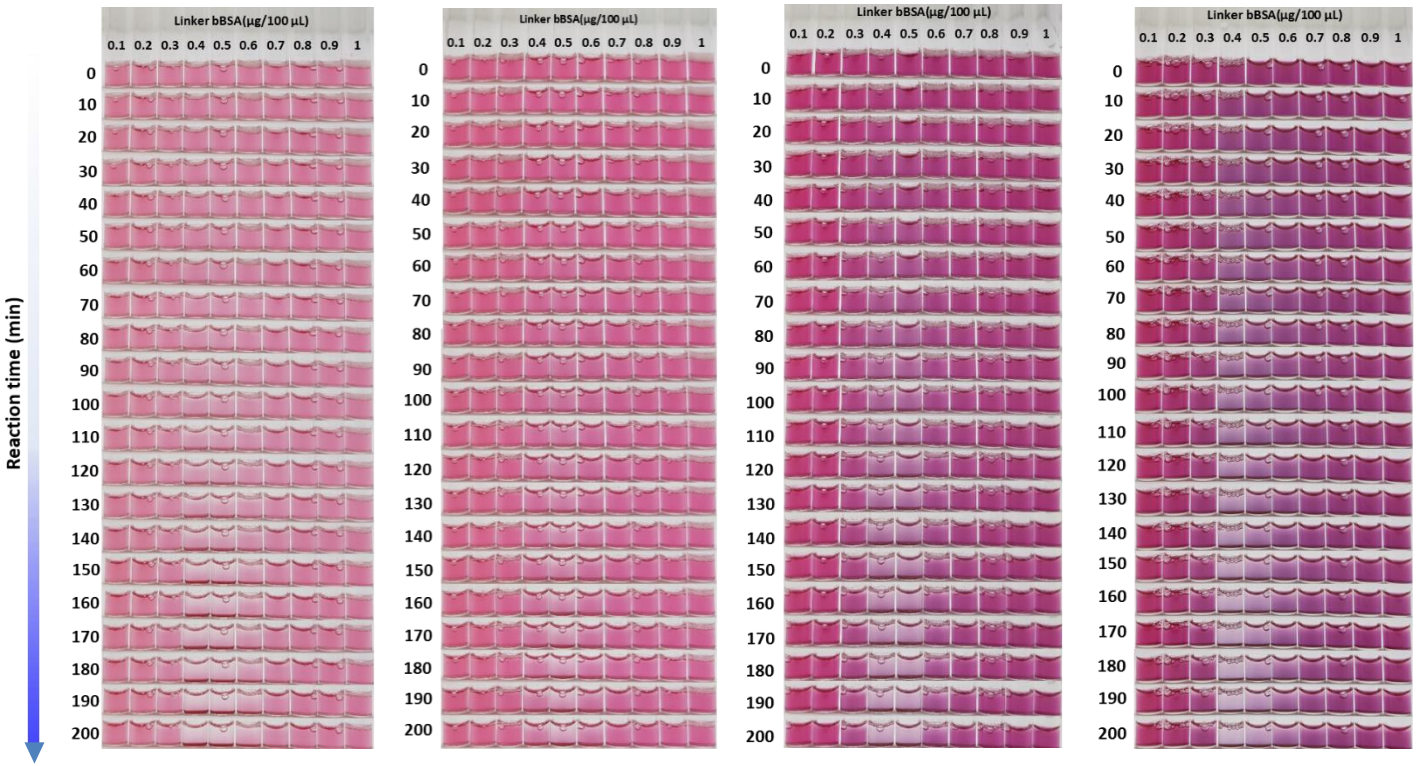

Figure 12. Images of REVC formation in 10 min intervals; (a) 13 nm, (b) 21 nm, (c) 30 nm, (d) 36 nm.

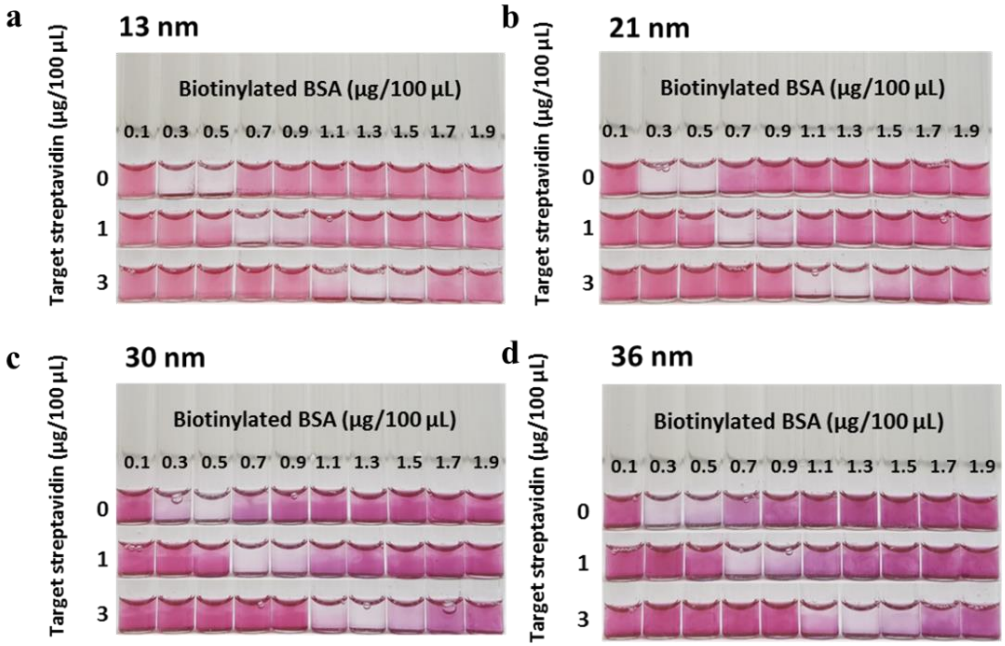

Figure 13. Images of REVC shifting depends on the different concentrations of target streptavidin addition; (a) 13 nm, (b) 21 nm, (c) 30 nm, (d) 36 nm.

3.2. Settling velocity of aggregates in REVC interpreted by the modified Stokes' law

Since REVC formation is a combined reaction of aggregation and precipitation, I focus on the basic mechanisms of colloidal aggregation and sedimentation phenomena. When particles are dispersed in colloid, they undergo Brownian motion (Allain, Cloitre, & Wafra, 1995; Aslan, Luhrs, & Pérez-Luna, 2004; Buzzaccaro, Tripodi, Rusconi, Vigolo, & Piazza, 2008; González, Odriozola, & Leone, 2004; Kovalchuk & Starov, 2012). Once particles aggregate and become large enough to settle under gravity, dominant movement in colloids change from diffusion to sedimentation (Batchelor, 1982; Langevin & Rondelez, 1978; Ohshima, 1998; Vesaratchanon, Nikolov, & Wasan, 2007). In the switchable-linker based aggregation system, rapid aggregation would be occurred because of a strong interaction between biotin (attached in linkers) and streptavidin (coated on the surface of AuNPs) (Weber, Ohlendorf, Wendoloski, & Salemme, 1989). Therefore, the key factors for reaction time would be the aggregation forming time and settling velocity.

3.2.1. Aggregates sizes obtained by DLS and TEM measurements of 13, 21, 30, and 36 nm-sized particles

Even though REVC appeared at similar linker concentrations under the same AuNPs surface area, there was a difference in precipitation time depends on the particle sizes (Figure 12). Particularly, within 200 min observation, REVC of 21 nm-sized particles seemed to be formed last. Since REVC forming time is critical as a sensor, verification of this phenomenon was achieved based on the aggregate sizes which was related to the settling velocity in REVC.

For the purpose of determining the sizes of aggregates in REVC, classic methods to identify the average particle sizes were carried out using DLS and TEM measurements. Also, spectrophotometer measurements were conducted since it has been well known that by measuring plasmon absorption peak (λ_{max}), approximate sizes of AuNPs could be expected (Haiss, Thanh, Aveyard, & Fernig, 2007). Based on the spectrophotometer data, λ_{max} gradually increased to a certain point and maintained constant in all the samples (Figure 14). According to the fact that increasing λ_{max} reflects the average particle sizes, I assumed that the sizes of aggregates in REVC increased to a certain point and aggregation slowed down once they grew large

enough. This can be explained by two reasons. First, as described above, in REVC, aggregation overlaps with precipitation, thus before aggregates reach a maximum size, precipitation was already under way. Secondly, in colloid system, the number of switchable linkers was limited, thus aggregates cannot be infinitely grown as time flows.

In addition to it, DLS measurements of aggregates on REVC as a function of time were conducted for all the samples (Figure 15). The obtained size data were hydrodynamic diameter of clusters which indicated the tendency most. The average sizes of aggregates in REVC decreased as the size of individual particles increased. I considered this phenomenon would be related to particles' Brownian motion in colloidal system. In TEM analysis, tendency of decreasing aggregate sizes was also observed (Figure 16-19).

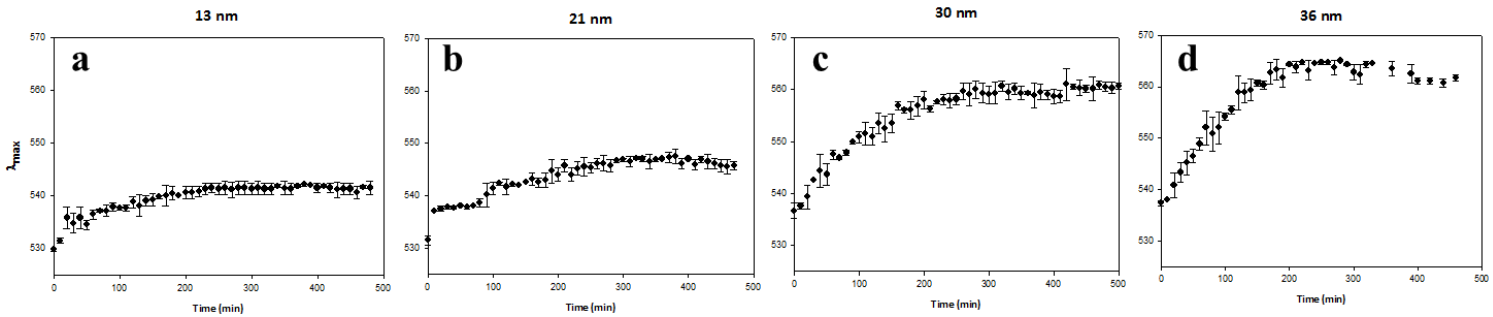

Figure 14. Changes in λ_{max} of aggregates on REVC as a function of time; (a) 13 nm, (b) 21 nm, (c) 30 nm, and (d) 36 nm.

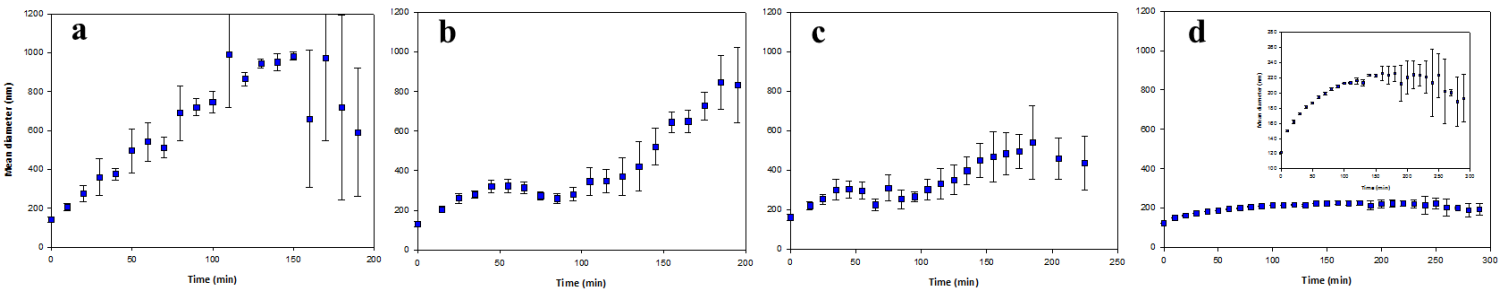

Figure 15. DLS measurements of mean diameter of aggregates on REVC as a function of time; (a) 13 nm, (b) 21 nm, (c) 30 nm, and (d) 36 nm. *All the data were based on hydrodynamic diameter.

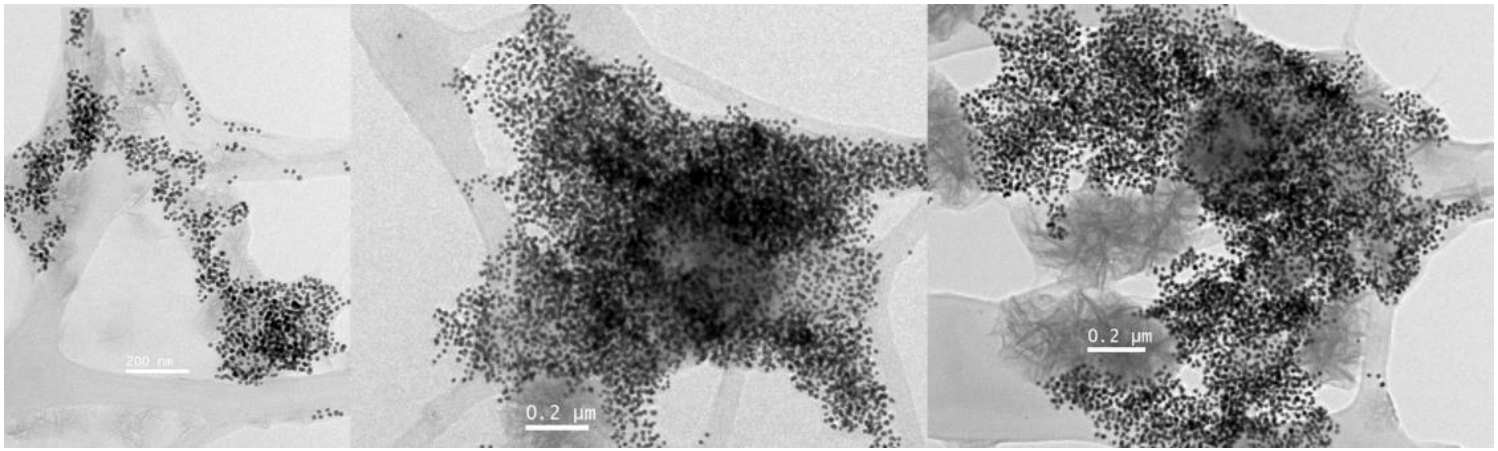

Figure 16. TEM images of aggregates on REVC - 13 nm.

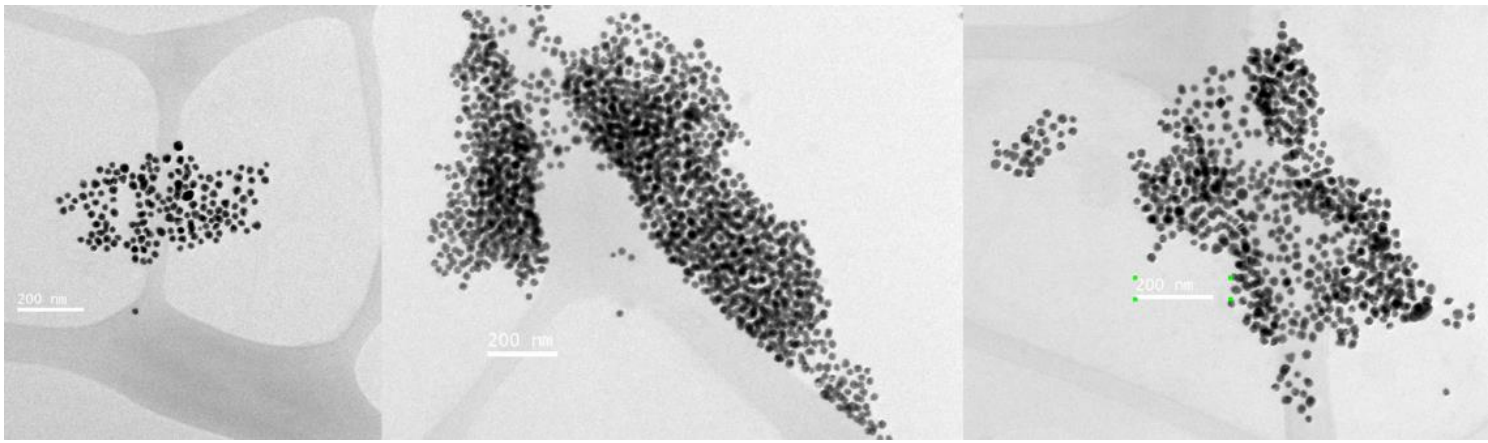

Figure 17. TEM images of aggregates on REVC - 21 nm.

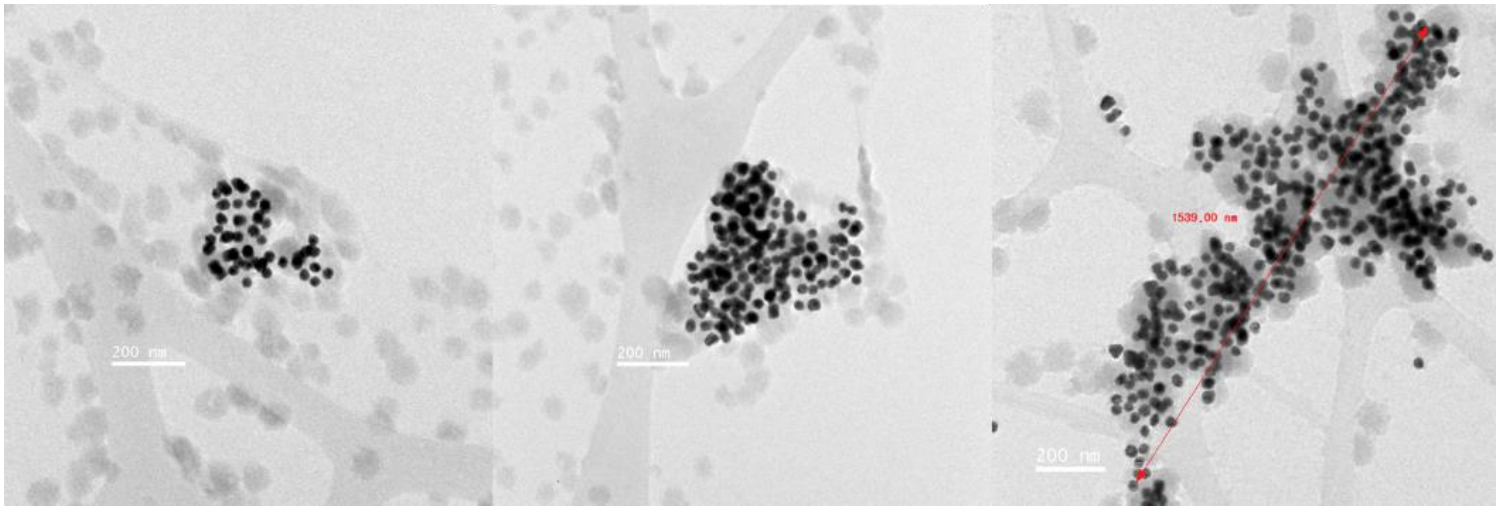

Figure 18. TEM images of aggregates on REVC - 30 nm.

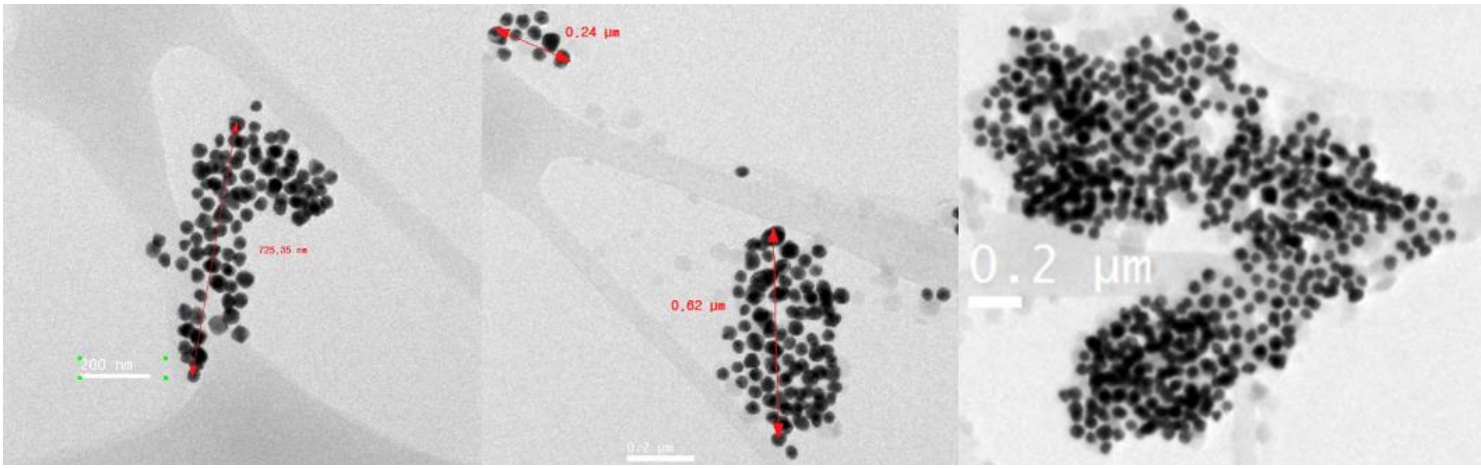

Figure 19. TEM images of aggregates on REVC - 36 nm.

3.2.2. Settling velocity of aggregates in REVC using the modified Stokes' law and occurrence of speed inversion phenomenon

The reaction in suspension during REVC formation is composed of particles aggregation and gravitational settling of aggregates. Aggregation and settling behavior of particles can be described by Brownian motion and Stokes' law, respectively. Since it is well known that particles' random Brownian motion can considerably disturb settling behavior, it is assumed that there would be a certain aggregate size that precipitation can occur (Ferguson et al., 2014). According to Figure 15, the aggregates were getting smaller as individual particle size increased, however, it was observed that in 30 and 36 nm sized particles, clusters precipitation occurred rather fast than 13 and 21 nm-sized particles and it is likely to say that the precipitation in 21 nm particle was the slowest among others as shown in Figure 12. This phenomenon might be due to the density difference of the aggregates, as shown in Figure 20. Assuming that in streptavidin-functionalized particles, the mass density of a cluster would be different depends on individual particle sizes. For example, density of a cluster made of 36 nm-sized particles was higher than that of 13 nm-sized particles, since the ratio of gold among the cluster would be bigger in cluster of 36 nm.

Calculations for the settling velocity of clusters were conducted as

follows. Each particle was assumed to be fully coated with streptavidin to exclude the effects of non-specific aggregation of particles, and the 3-dimentional size of streptavidin was considered approximately as ~4.5 x 4.5 x 5.8 nm (Weisenhorn, Schmitt, Knoll, & Hansma, 1992). The density of gold was 19.32 g/cm^3 (Brown & LeMay, 1985), amount of streptavidin coated on the surface of AuNPs was cited by the previous research using BSA, since the dimension of the proteins are similar (Brewer, Glomm, Johnson, Knag, & Franzen, 2005). The amount of streptavidin for AuNPs surface coverage was considered as 3.7 x 10 ^{12} molecules/cm^2 (Brewer et al., 2005). The molecular weight of streptavidin was 52.8 kDa (Panchapakesan, Jeng, & Unrau, 2015). The total volume of the streptavidin-functionalized particles was calculated considered streptavidin diameter as 2.5 nm since proteins are known to be spread making themselves smaller when they are attached to the metal surface, and the used equation was as follows [1], where D*p* represents diameter of AuNPs.

$$V = \frac{4}{3}\pi\left\{\frac{(D_p+5)}{2}\right\}^3 \qquad [1]$$

The total mass of streptavidin-functionalized AuNPs was calculated as the sum of M_g and M_s, which represent mass of single gold nanoparticle and mass of

total streptavidin coated on the surface of a gold nanoparticle. Finally, the density of single particle was calculated dividing mass by volume.

The modified Stokes' law was used to fully reflect the settling velocity of gold clusters having specific fractal dimension with the following equation [2].

$$v_{sed} = \frac{2(\rho_s - \rho_m)gNr^3}{9\mu R_g} \qquad [2]$$

Where ρ_s and ρ_m are the densities of gold (19,320 kg m^{-3}) and medium (1000 kg m^{-3}), respectively. g represents the gravitational force (9.8 m s^{-2}), N is the number of nanoparticles per aggregate, r is the radius of AuNPs (m), μ is the viscosity of the medium (1.4 x 10-3Pa s) and R_g is the radius of gyration (m) which is the size of clusters. For the R_g value, gold fractal dimension of 1.75 was considered (Albanese & Chan, 2011). In this case, size of aggregates was obtained based on the DLS number based data, since the massive tendency of aggregates is important in the system.

Settling velocity of clusters made of 4 different sized particles within 120 min was as shown in Figure 21. Since aggregates became larger than 1000 nm, which far beyond the mechanical measurement limit, measurements took

place within 120 minutes. At an early stage, settling velocity of 30 and 36 nm-sized particles was faster than that of 13 and 21 nm-sized particles. Settling speed of 13 nm-sized particles constantly increased and at around 120 min, the speed reached over the 21 nm-sized particles. Higher density of clusters made up of 30 and 36 nm particles, resulting in faster settling of aggregates in the beginning, it seemed like 13 nm particles formed aggregates desirably in much bigger sizes ended up accelerating the settling velocity as time went by. Overall, it was revealed that setting speed could be affected by the various factors which were related to the aggregation.

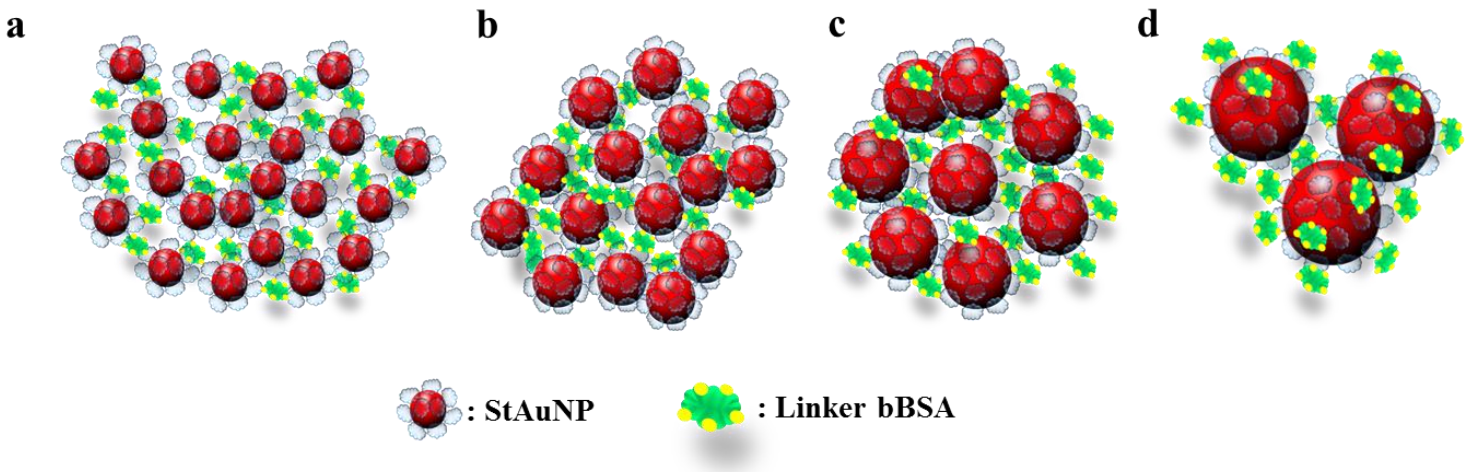

Figure 20. Schematic of aggregates in REVC upon size of individual AuNPs: (a) 13 nm, (b) 21 nm, (c) 30 nm, and (d) 36 nm.

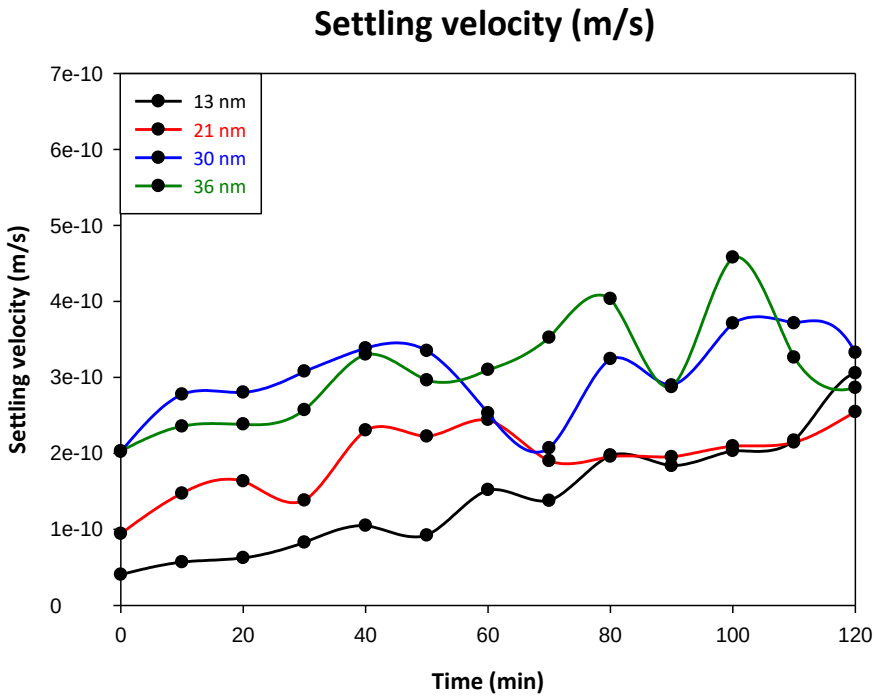

Figure 21. Settling velocity of aggregates in REVC within 120 minutes.

IV. CONCLUSION

In this study, the effects of AuNPs surface area on REVC formation were verified using 3 different conditions. When the plasmon absorbance was identically adjusted using 11 and 19 nm nanoparticles, REVC showed up at lower linker concentrations with narrower range which acted more sensitively as a sensor. Under the addition of target streptavidin, 19 nm particles acted more sensitively. When the number of particles was equally matched using 12, 18, and 24 nm particles, REVC appeared at higher linker concentrations with broader range as the size of particle increased. This result was ultimately same with that of the previous condition. And REVC shifted less as the surface area of particles increased from 12 to 24 nm. Lastly, when the surface area of particle in the size of 13, 21, 30, and 36 nm was identically adjusted, REVC appeared at similar linker concentrations. REVC shifting occurred in the similar extent regardless of particle sizes. All of three cases showed that AuNPs surface area significantly affected in the formation of REVC, and as the surface area decreased it acted more sensitively as a sensor.

In addition, the properties of aggregates in REVC in terms of settling velocity under the same surface area with 4 different sized particles were studied. It was observed that in 21 nm sized particles, REVC formation was

slower than other sized particles. Thus, based on the DLS size measurements of aggregates and modified Stoke's law, the settling velocity of gold nanoparticles clusters in REVC was calculated within 120 minutes. At an early settling stage, settling velocity of larger particles, which were 30 and 36 nm size was faster compared to smaller particles. As time went by, the precipitation velocity of 13 nm size became faster than that of 21 nm particles, and eventually reached over that of 30 and 36 nm sized particles. This settling velocity inversion phenomenon could be occurred according to the relationship of aggregates size, individual nanoparticle size, the number of particles per aggregate, and viscosity difference between aggregates and fluid, based on the modified Stokes' law.

This research can be used as a basic study of factors that affect REVC formation in the switchable-linker based detection system and contributed to the development of the system.

V. REFERENCES

Ai, K., Liu, Y., & Lu, L. (2009). Hydrogen-bonding recognition-induced color change of gold nanoparticles for visual detection of melamine in raw milk and infant formula. *Journal of the American Chemical Society, 131*(27), 9496-9497.

Albanese, A., Chan, W. (2011). Effect of gold nanoparticle aggregation on cell uptake and toxicity. *ACS nano*, 5(7), 5478-5489.

Allain, C., Cloitre, M., & Wafra, M. (1995). Aggregation and sedimentation in colloidal suspensions. *Physical review letters, 74*(8), 1478.

Aslan, K., Luhrs, C. C., & Pérez-Luna, V. H. (2004). Controlled and reversible aggregation of biotinylated gold nanoparticles with streptavidin. *The Journal of Physical Chemistry B, 108*(40), 15631-15639.

Batchelor, G. (1982). Sedimentation in a dilute polydisperse system of interacting spheres. Part 1. General theory. *Journal of Fluid Mechanics, 119*, 379-408.

Brewer, S. H., Glomm, W. R., Johnson, M. C., Knag, M. K., & Franzen, S. (2005). Probing BSA binding to citrate-coated gold nanoparticles and surfaces. *Langmuir, 21*(20), 9303-9307.

Brown, T. L., & LeMay, H. E. (1985). Qualitative inorganic analysis: to accompany Chemistry, the central science: Prentice Hall.

Buzzaccaro, S., Tripodi, A., Rusconi, R., Vigolo, D., & Piazza, R. (2008). Kinetics of sedimentation in colloidal suspensions. *Journal of Physics: Condensed Matter, 20*(49), 494219.

Ferguson, J., Schultz, B. F., Rohatgi, P. K., & Kim, C.-S. (2014). Impact of Brownian motion on the particle settling in molten metals. *Metals and Materials International, 20*(4), 747-755.

Fischer, H., Polikarpov, I., & Craievich, A. F. (2004). Average protein density is a molecular-weight-dependent function. *Protein Science, 13*(10), 2825-2828.

González, A., Odriozola, G., & Leone, R. (2004). Colloidal aggregation with sedimentation: concentration effects. *The European Physical Journal E, 13*(2), 165-178.

Hahn, J., Kim, E., You, Y. S., Gunasekaran, S., Lim, S., & Choi, Y. J. (2017). A switchable linker-based immunoassay for ultrasensitive visible detection of *Salmonella* in Tomatoes. *Journal of food science, 82*(10), 2321-2328.

Haiss, W., Thanh, N. T., Aveyard, J., & Fernig, D. G. (2007). Determination of size and concentration of gold nanoparticles from UV− Vis spectra. *Analytical chemistry, 79*(11), 4215-4221.

Kovalchuk, N., & Starov, V. (2012). Aggregation in colloidal suspensions: Effect of colloidal forces and hydrodynamic interactions. *Advances in colloid and interface science, 179*, 99-106.

Langevin, D., & Rondelez, F. (1978). Sedimentation of large colloidal particles through semidilute polymer solutions. *Polymer, 19*(8), 875-882.

Lim, S., Koo, O. K., You, Y. S., Lee, Y. E., Kim, M.-S., Chang, P.-S., . . . Gunasekaran, S. (2012). Enhancing nanoparticle-based visible detection by controlling the extent of aggregation. *Scientific reports, 2*, 456.

Liu, R., Chen, Z., Wang, S., Qu, C., Chen, L., & Wang, Z. (2013). Colorimetric sensing of copper (II) based on catalytic etching of gold nanoparticles. *Talanta, 112*, 37-42.

Nath, N., & Chilkoti, A. (2002). A colorimetric gold nanoparticle sensor to interrogate biomolecular interactions in real time on a surface. *Analytical chemistry, 74*(3), 504-509.

Ohshima, H. (1998). Sedimentation potential in a concentrated suspension of spherical colloidal particles. *Journal of colloid and interface science, 208*(1), 295-301.

Panchapakesan, S. S. S., Jeng, S. C., & Unrau, P. J. (2015). RNA complex purification using high-affinity fluorescent RNA aptamer tags. *Annals of the New York Academy of Sciences, 1341*(1), 149-155.

Shrivas, K., Shankar, R., & Dewangan, K. (2015). Gold nanoparticles as a localized surface plasmon resonance based chemical sensor for on-site colorimetric detection of Arsenic in water samples. *Sensors and Actuators B: Chemical, 220*, 1376-1383.

Vesaratchanon, S., Nikolov, A., & Wasan, D. T. (2007). Sedimentation in nano-colloidal dispersions: effects of collective interactions and particle charge. *Advances in colloid and interface science, 134*, 268-278.

Vilela, D., González, M., & Escarpa, A. (2012). Sensing colorimetric approaches based on gold and silver nanoparticles aggregation: Chemical creativity behind the assay. A review. *Analytica chimica acta, 751*(751), 24-43.

Wang, Z., Lee, J. H., & Lu, Y. (2008). Label-free colorimetric detection of lead ions with a nanomolar detection limit and tunable dynamic range by using gold nanoparticles and DNAzyme. *Advanced Materials, 20*(17), 3263-3267.

Weber, P. C., Ohlendorf, D., Wendoloski, J., & Salemme, F. (1989). Structural origins of high-affinity biotin binding to streptavidin. *Science, 243*(4887), 85-88.

Weisenhorn, A., Schmitt, F.-J., Knoll, W., & Hansma, P. (1992). Streptavidin binding observed with an atomic force microscope. *Ultramicroscopy, 42*, 1125-1132.

Zhao, W., Ali, M. M., Aguirre, S. D., Brook, M. A., & Li, Y. (2008). based bioassays using gold nanoparticle colorimetric probes. *Analytical chemistry, 80*(22), 8431-8437.

국문초록

특이적인 광학적 성질을 나타내는 금나노 입자의 응집반응은 특정 타겟 물질을 검출하기 위하여 다양한 분야에서 널리 사용되고 있다. 선행연구에서는 switchable-linker기반 금나노 입자의 응집반응을 이용하여 살모넬라와 알러젠 Ara h1의 검출이 이루어졌지만, 시스템에서 링커와 금나노 입자가 연결되어 최대한의 응집이 일어나고 응집체의 침강이 이루어지는 구간(REVC) 형성에 영향을 미치는 요소와 시스템 내 금나노 입자의 응집과 침강 반응에 관한 기초연구는 미비한 실정이다.

본 연구에서는 금나노 입자의 표면적이 REVC형성에 미치는 영향을 알아보고자 세 가지 조건에서 실험을 진행하였다. 첫째, 흡광도를 0.4로 동일하게 맞춘 11 nm 와 19 nm 크기의 금나노입자의 경우, REVC는 더 낮은 linker농도에서 나타났으며, 형성되는 REVC의 범위는 좁아졌다. REVC의 범위가 좁을수록 linker 농도에 더욱 민감하게 반응한다는 의미이므로 센서로서 바람직한 현상이다. Target으로 streptavidin을 넣었을 때, 같은 양의 target에 대하여 표면적이 더 작은 19 nm 크기의 입자에서 control대비 더 많

은 shifting이 일어나 target에 더욱 민감하게 반응하는 것을 확인하였다. 둘 째, 12, 18, 24 nm 크기 금나노 입자의 단위 부피당 개수를 모두 동일하게 맞추어 주었을 때, REVC는 표면적이 가장 작은 12, 18, 24 nm 순으로 더 낮은 linker영역대에서 형성되었고, 형성되는 REVC의 영역 역시 좁았다. Target streptavidin을 넣어주었을 때, 표면적이 더 작은 12, 18, 24 nm 순으로 control 대비 shifting이 잘 일어났다. 마지막으로, 13, 21, 30, 그리고 36 nm 사이즈의 금나노 입자 표면적을 모두 동일하게 조절하였을 때, REVC는 네 크기의 입자 모두 동일한 영역에서 REVC가 형성되었다.

이 때, 특이적으로 21 nm크기의 입자에서 REVC형성이 느려지는 현상을 목격하였고, 이에 대해 REVC에서 형성되는 응집체들의 평균 크기와 침강속도와의 관계를 변형된 Stokes' law를 이용해 규명해보고자 하였다. REVC에서 형성된 13, 21, 30, 그리고 36 nm 입자의 응집체의 크기를 시간에 따라 DLS로 측정하였고, 금나노 입자가 클러스터를 형성할 때 1.75 치의 프랙탈 차원 값을 갖는다는 점을 염두하여 입자와 유체의 밀도차, 응집체를 구성하는 입자의 수, 구성하는 금나노 입자의 크기, 그리고 평균 응집체의 크기를 반영한 변형된 Stokes' law를 이용하여 침강 될 때의 종말

속도를 구하였다. 그 결과, 침강 초반 30 nm 와 36 nm 의 응집체의 침강속도가 빨랐으며, 13 nm 와 21 nm 응집체의 침강속도는 서서히 30 nm 와 36 nm 침강속도를 따라잡았다. 120 분 부분에서는 13 nm 응집체가 21 nm 응집체의 침강속도를 넘어서는 현상을 발견하였는데, 이는 시각적 현상으로 발견한 침강속도 역전 현상과 부합하는 결과였다. 본 연구자는 이와 같은 현상에 DLS와 TEM측정을 통해 금나노 입자의 크기가 커질수록, 형성되는 응집체가 작아진다는 결과를 참고하여, 크기가 작은 입자들은 빠르게 응집하여 더 큰 크기의 응집체를 형성하게 되고, 그에 따라 침강속도 역시 시간이 지남에 따라 빠르게 증가하기 때문일 것이라고 사료하였다.

본 연구는 switchable linker기반 검출법에서 가장 중요한 REVC형성에 대하여 입자의 표면적이 주요한 요소임을 제시하였고, 응집체의 크기에 따른 침강속도의 역전현상이 발생할 수 있다는 사실을 확인하였다. 이는 추후 시스템에서 반응 속도와 민감도 부분을 개선하는데 기여하고 식품 산업에서 사용될 수 있는 센서로서의 기반을 다지는 기초연구로서 의의를 갖는다.

주요어: 금나노 입자, REVC, switchable linker, 크기, 반응표면적, 응집, 침강,

학번: 2016-25275